

7.5

Hourly convective probability forecasts and experimental high-resolution predictions based on the radar reflectivity assimilating RUC model

Stephen S. Weygandt¹, Stanley G. Benjamin¹, Tatiana G. Smirnova^{1,2},
John M. Brown¹, and Kevin Brundage^{1,3}

¹NOAA Earth System Research Laboratory, Global Systems Division, Boulder, CO, USA

²Cooperative Institute for Research in Environmental Sciences (CIRES), Boulder, CO, USA

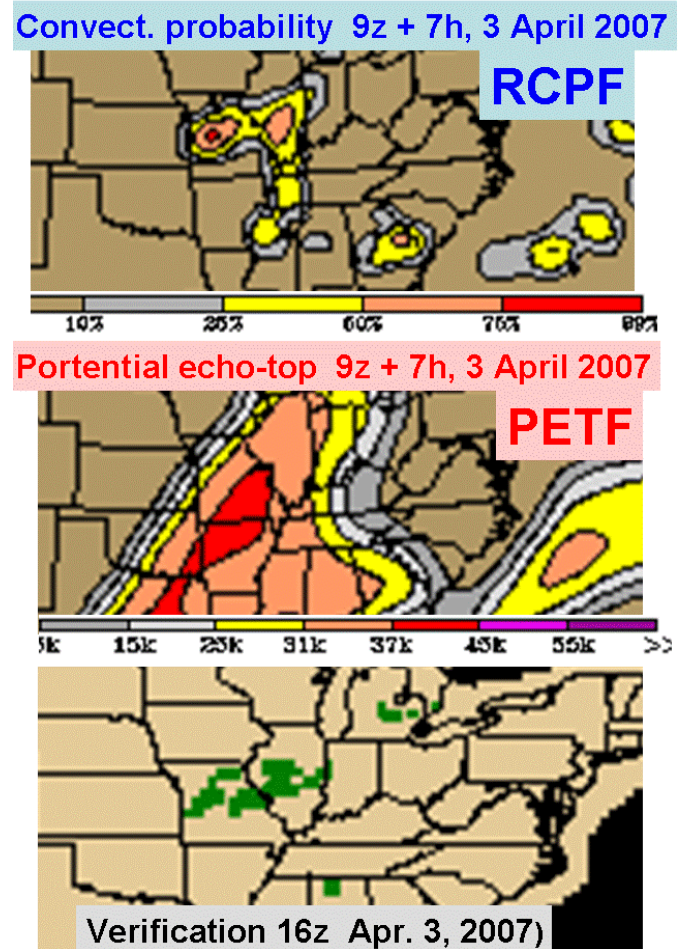
³Cooperative Institute for Research in the Atmosphere (CIRA), Fort Collins, CO, USA

1. Introduction

For the past four years, The ESRL Global Systems Divisions has produced probabilistic thunderstorm likelihood forecasts by applying statistical post-processing techniques to time-lagged ensembles of Rapid Update Cycle (RUC) model output. Since March of 2005, these forecasts have been distributed in real-time to the Aviation Weather Center (AWC) and other users. At AWC, the products have provided guidance to humans, who prepare various convective forecasts, including the Collaborative Convective Forecast Product (CCFP). These RUC-based convective forecasts have continued to evolve and new features have been added. Currently two specific products, the RUC Convective Probability Forecast (RCPF) and Potential Echo Top Forecast (PETF) are being created with hourly updates and hourly output to 10-h.

As detailed in Weygandt et al. (2004), the RCPF is created by utilizing adjacent gridpoints and time-lagged RUC ensemble members to calculate the fraction of gridpoints with convective precipitation exceeding a diurnal and regionally varying threshold. The PETF utilizes RUC environmental sounding information averaged over adjacent gridpoints and time-lagged ensembles to provide a conditional (assuming convection occurs) estimate of the potential echo top in thousands of feet. Fig. 1 provides an illustration of the products and comparison with a 40-km depiction of the NCAR National Convective Weather Diagnostic (NCWD) used for verification of the RCPF. As can be seen, the convective probabilities are found within a larger region potential echo-top region, where the time-lagged ensemble model guidance

from the RUC indicates convection is possible. Note the regions outside the lowest echo-top contour (5,000 feet) generally correspond to areas with no convective available potential energy (CAPE), and thus convection is very unlikely.



* Corresponding author address: Steve Weygandt,
NOAA/GSD, R/E/GSD, 325 Broadway, Boulder,
CO 80305 stephen.weygandt@noaa.gov

Fig. 1. Illustration of RUC Convective Probability forecast (RCPF) and Potential Echo-Top Forecast (PETF) products for 7-h forecast valid 16z April 2007.

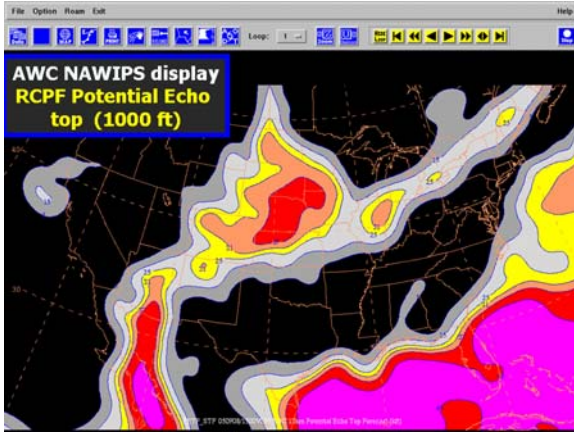


Fig. 2. Potential Echo-Top Forecast (PETF) product as it appears on the Aviation Weather Center (AWC) workstation.

As noted above, the hourly RCPF and PETF files are being transmitted to AWC for use by convection forecasters. To fully utilize the products, forecasters must be able to integrate the RCPF and PETF fields with other guidance products, which is accomplished by displaying the fields on the AWC forecaster workstations, where other information can be overlaid. Fig. 2 shows a sample depiction of the PETF on the workstation.

2. Evolution of the RCPF

The RCPF has undergone a continual refinement process since its inception in 2003. Principal improvements have been optimizing the probabilities based on adjustments to specific parameter values, addition of the potential echo-top product, and use of time-lagged ensembles from the RUC. In this section we first describe the adjustments to the parameter values, which is effectively a bias correction, then discuss the use of time-lagged ensembles.

2.1 OPTIMIZING THE PROBABILITIES

Weygandt et al (2004) describe in detail a procedure for creating a convective probability forecast at any point, based on the fraction of model gridpoints within a specific distance that are forecast to have convective precipitation exceeding a specific threshold. This approach follows work described by Germann and Zawadzki (2002, 2004). For our application, the character of the convective probabilities is strongly impacted by the choice of two parameters: 1) the spatial filter size and 2) the convective precipitation threshold. For radar data

advection nowcasting applications, the optimal spatial length scale should increase with time, as predictability is lost for progressively larger spatial scales as lead-time is increased (Germann and Zawadzki 2002, 2004). In addition, as documented by Ajevich et al., there are strong diurnal and regional convective patterns, and that statistical information on these patterns can be used to optimize the probability. Based on empirical testing and evaluation for the specific RCPF application, we have built in some crude aspects of this diurnal and regional information.

Specifically, a forecast lead-time invariant filter size of 9 RUC (13-km) gridpoints (+/- 4 points) was selected for the longitudes east of 104 degrees, and 7 RUC gridpoints (+/- 3 points) for longitudes west of 104 degrees. The lead-time invariance is at odds with results from pure radar data-based nowcast algorithms, and likely reflects the model spin-up issues. In contrast to radar advection algorithms (for which skill is initially very high, then gradually declines), for model-based forecast systems, without radar or precipitation assimilation schemes, forecast skill is typically poor for the first few hours, as the precipitation systems “spin-up” within the model. This spin-up problem can be significantly mitigated by use of a radar assimilation procedure as described in section 3.1. The model spin-up issue also has implications for the use of time-lagged ensembles, as will be discussed in section 2.2. The crude regional variation to the spatial filter size was empirically determined and reflects the smaller-scale nature of convection and lack of large propagating MCSs in the western CONUS. The algorithm could likely be further improved by building in a terrain-related aspect, especially in the western U.S., where afternoon convection is strongly correlated with terrain features.

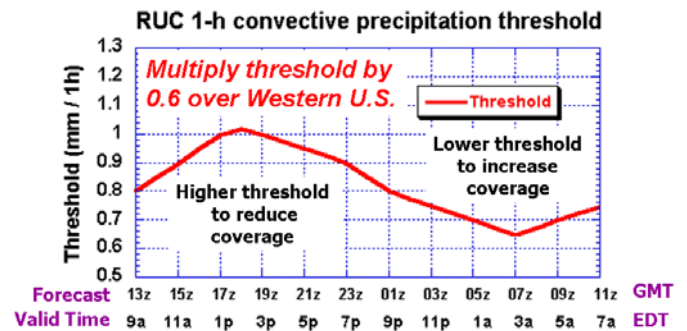


Fig. 3. Diurnally varying convective precipitation threshold

A regionally varying strong diurnal pattern obviously also exists for convective activity. This again has been crudely addressed by imposing a diurnally (based on the forecast valid time) varying convective precipitation threshold to the RCPF algorithm. As shown in Fig. 3. Noting that for the RUC, we have based the RCPF on the convective (model parameterized) precipitation, this diurnal adjustment represent an adjustment to compensate for the model overprediction of convective precipitation during the day and underprediction of convective precipitation during the night. As indicated in the fig. a simple regional variation is also added to reflect the reduced precipitation amounts typically found in western convection.

2.2 USE OF TIME-LAGGED ENSEMBLES

Because the RUC model system ingests new observations and produces a new forecast each hour with hourly output out to 12-h, it provides a low-cost opportunity to utilize time-lagged ensemble techniques for the RCPF and a host of other probabilistic forecasts. While time-lagged ensembles can be expected to exhibit a higher degree of correlation (less degrees of freedom) than ensembles generated by some other techniques, they have proven to be beneficial for the RCPF

generation. In addition, we have experimented with time-lagged ensembles for probabilistic ceiling forecasts. Since 2004, we have augmented the spatial filtering approach used for generating convective probabilities with the use of time-lagged ensemble members.

Fig. 4 provides an overview of the methodology for the time-lagged ensembles and gives specific information on forecasts used for a specific time. For the GSD real-time RUC cycle used to create the RCPF, there is a 2-h latency for the 12-h forecast (note for the operational RUC there is only a 1-h latency for the 12-h forecast). Thus, for a given available time (15z in Fig. 4), we can use RUC forecasts from 2 h previous and older. (13z and older). Because the 1-h RUC convective precipitation represents an accumulation for the previous hour ending at the valid time, the use of two adjacent hourly convective precipitation totals from each RUC model run will provide a 2 hour bracketing period centered on the valid time, as shown in Fig. 4. Thus, by considering 2 successive hourly sums for each model run and successively older model runs, we arrive (for each valid time) at the “model outputs used” as shown in the boxes in Fig. 4.

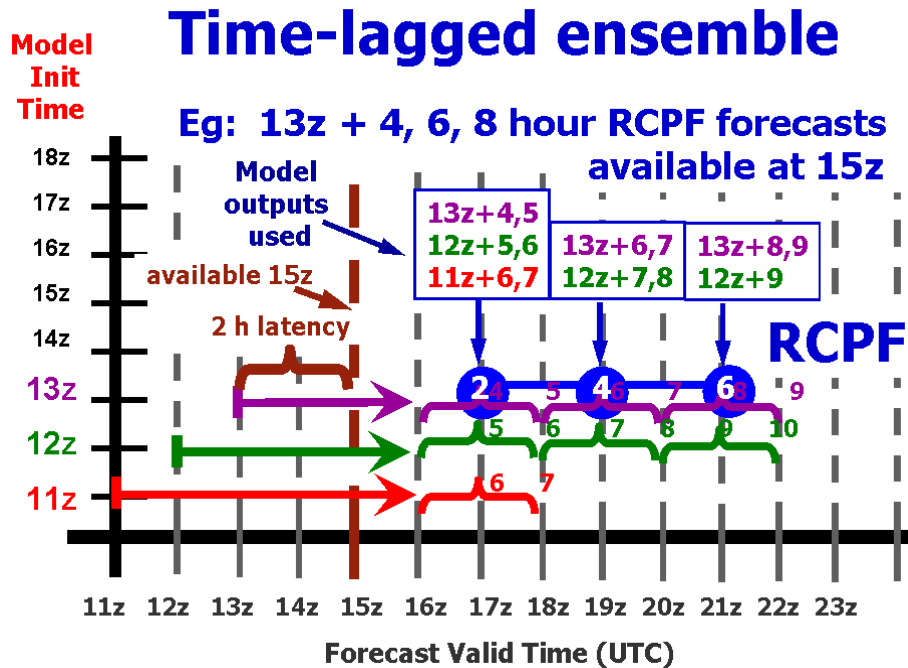


Fig. 4. Flow chart illustrating the process by which time-lagged deterministic RUC ensemble members are used to create the RCPF. For a given forecast available time (15z) the specific RUC model runs and output times used are shown for the different RCPF forecast lengths. The role of 2-h product latency in determining which runs can be used is also shown.

In 2004, we conducted a comparison of RCPF forecasts with and without the use of time-lagged ensembles and CCFP forecasts (verified against the 40-km NCWD). The results, summarized in Figs. 5 and 6, illustrate a number of interesting aspects to both the automated and human produced forecasts. Shown in Fig. 5 is a contour plots of the CSI as a function of two parameters, forecast lead-time (vertical axis) and forecast valid time (horizontal axis). Presentation of the scores in this format provides an encompassing illustration that highlights key characteristics. The color band progression from grey, through blue, through pink, then yellow depicts increasingly superior CSI scores. Note that the top contour plot (“RCPF v2003”, “NO time-lag”) was the original 2003 formulation without the time lag, run in a frozen state for the August 2004 test period indicated. The middle contour plot (“RCPF v2004”, “Time-lag”) was the then current 2004 version with use of time-lagged ensembles. In 2004, with shorter forecast

length and no product dissemination to AWC, there was only a 1-h latency. Thus 3-, 5, and 7-h RCPFs were compared with 2, 4, and 6-h CCFPs. Lastly, note the bottom curve indicating the diurnal cycle of convective coverage as depicted by the fraction of the domain covered by 40-km NCWD convective boxes. This curve is key, as much of the interpretation of the results will focus on diurnal skill variations relative to this diurnal convective coverage cycle. Fig. 6, shows the corresponding contour plots for the bias scores, with pink colors indicating a low bias relative to the 40-km NCWD and blue to yellow, to green indicating increasingly high biases.

First, note the strong overall similarity between the CSI patterns for all three forecasts. As expected, skill is strongly peaked for forecast valid in the afternoon when convection is most active. Key differences between the RCPF and CCFP are apparent, however, with the CCFP forecast skill improving significantly as forecast lead-time

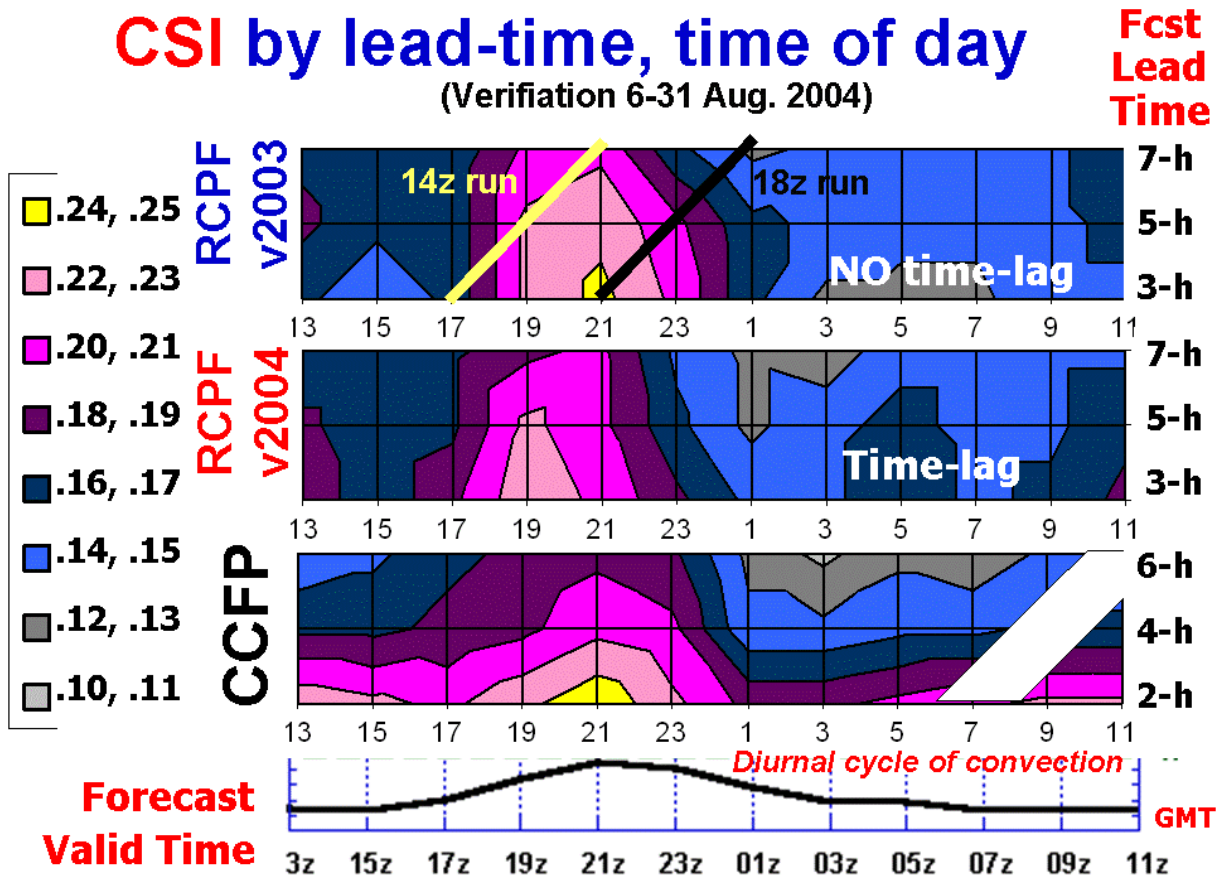


Fig. 5. Contour plot of CSI as a function of forecast lead-time (vertical axis) and forecast valid time (horizontal axis) for the RCPF without using time-lagged ensembles (top panel), RCPF with use of time-lagged ensembles (middle panel), and the CCFP (bottom panel). The diurnal cycle of observed convective coverage is also shown along the bottom.

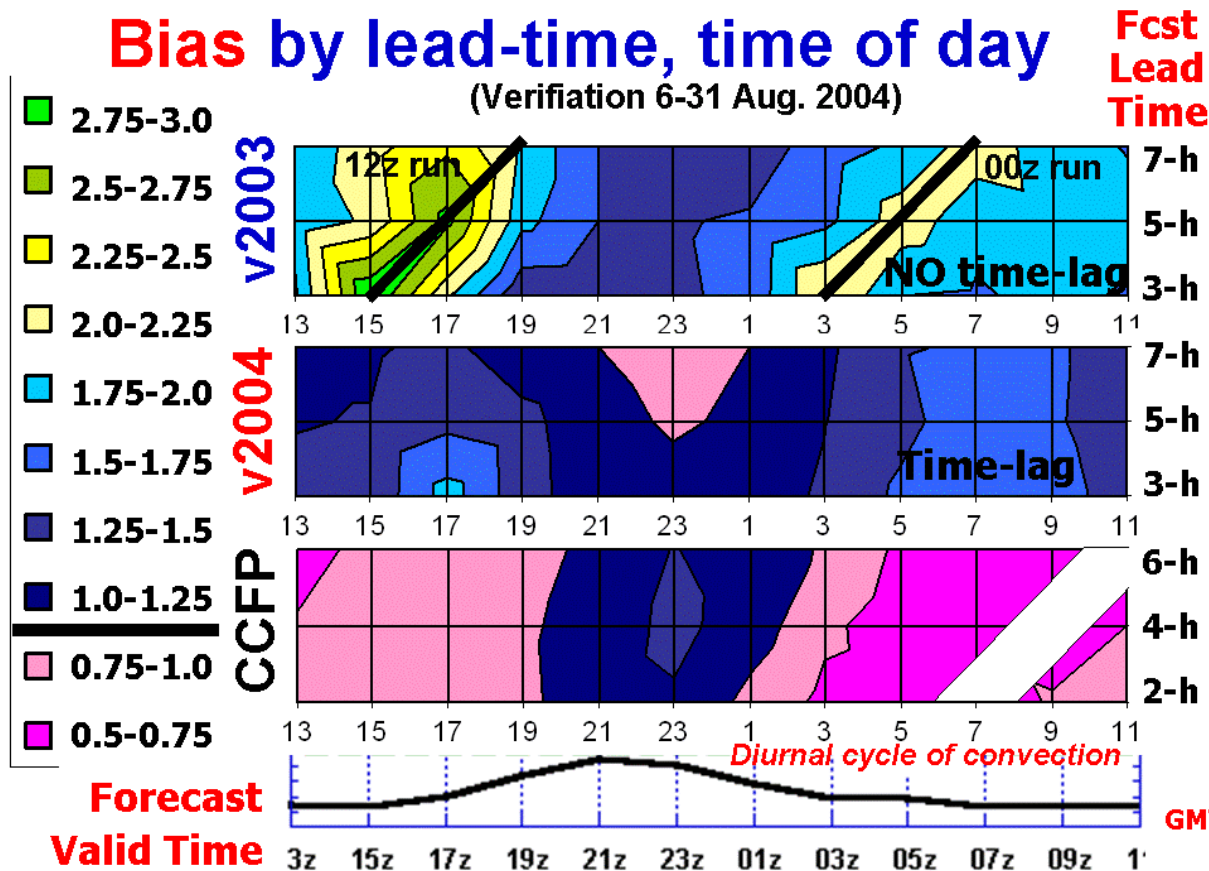


Fig. 6. Contour plot of bias as a function of forecast lead-time (vertical axis) and forecast valid time (horizontal axis) for the RCPF without using time-lagged ensembles (top panel), RCPF with use of time-lagged ensembles (middle panel), and the CCFP (bottom panel). The diurnal cycle of observed convective coverage is also shown along the bottom.

decreases and the forecast skill improvement occurring a bit earlier in the day for the RCPF forecasts. There is also an important (and related) difference in the diurnal bias cycle, with the CCFP bias increasing during the day, while the RCPF bias decreases during the day. Also, the RCPF biases are more vertically aligned, indicating they are a strong function of valid time, not initial time. In contrast, the CCFP biases are more diagonally aligned, indicating they are a function of forecast time as well as valid time. Taken as whole, these patterns suggest that the RCPF forecasts depict a more time invariant amount of convection, whereas, for the CCFP forecasts, the amount of forecast convection increases even more than the actual convection increase during the day.

Comparison of the CSI for the two RCPF versions reveals the impact of the time-lagged ensemble in mitigating the effects of the model spin-up problem. Note, first that for the “NO time-lagged” case, values along a 45 degree diagonal (depicted by the tan and black lines) represent scores for a specific RUC run (model initialization

time). Examination of the 14z forecast (diagonal tan line in Fig. 4) shows that the average forecast skill actually increases from the 3-h to the 5-h forecast. This pattern, which also occurs through much of the night is likely due to the model spin-up problem. In contrast, the 18z forecast (diagonal black line in Fig. 4) shows a steady decrease in forecast skill from the 3-h to the 7-h forecast.

With this understanding, the process of including time-lagged ensembles (the middle panel in Fig. 4) can be illustrated as averaging in older forecasts (averaging “upwards” in the top panel). Thus at time of the day when the model spin-up problem is more pronounced (overnight through morning) we would expect forecast improvement from the time-lagged ensemble. At times when the model spin-up problem is a minimum (afternoon), we would expect some degradation of the forecast skill from the time-lagged ensemble. Comparison of the top two panels in Fig. 5, indicates that this is in fact generally true. The concept of a diurnal cycle to the degree of model spin-up problem is consistent with the notion that during the afternoon,

the boundary layer is well heated and convective inhibition is minimized. This also suggests that it may be beneficial to diurnally vary the degree to which time-lagged ensembles are used. Finally, we note the strong diagonal tendency in the bias field for the “No Time-lag” RCPF. This is apparently related to the extra excitation of the cumulus parameterization at the radiosonde initialization times. We have not seen this in precipitation verification of RUC forecasts and it was significantly improved by the use of time-lagged ensembles. This illustrates an additional important benefit of the time-lag ensemble, a much greater time continuity between successive RCPF forecasts. This is extremely important to forecasters using guidance products and has been the subject of verification by Kay et al (2006).

3. Summer 2007 Activities

A number activities related to the RCPF and RUC-based convective guidance occurred during the summer of 2007. First, a radar reflectivity assimilation procedure was successfully included within the RUC prediction system and is slated for operational implementation at NCEP later in 2008. This procedure is described in detail in companion papers (Weygandt et al. 2008 and Benjamin et al. 2008), and will be briefly summarized here. This new capability to initialize ongoing convective systems directly addresses the model spin-up problem, leading to improved RUC deterministic forecasts and improved RCPF forecasts. Work to incorporate a related change to the RCPF to further capitalize on the radar assimilation is underway. Second, the RCPF (as well as RUC predicted simulated reflectivity) was included in an operationally oriented quantitative and subjective verification program. We will present here the verification statistics available to us and some specific case examples.

Third, we began experimental High Resolution Rapid Refresh (HRRR) 3-km (explicit convection resolving) simulations on a small northeast corridor domain. These runs were initialized from the RUC version that included the radar reflectivity assimilation on the 13-km. Selected results and comparisons of HRRR runs initialized from the RUC versions with and without the radar assimilation will be shown to illustrate the importance of the radar reflectivity assimilation on the 13-km RUC grid for improving the subsequent 3-km HRRR convective prediction.

3.1 RUC REFLECTIVITY ASSIMILATION

The new RUC radar reflectivity assimilation procedure utilizes two existing RUC system components, the cloud analysis and the diabatic digital filter initialization (DDFI), to prescribe during the pre-forecast integration a specified temperature tendency (warming) within the radar-observed reflectivity regions. This temperature tendency is deduced as a latent heating rate from the radar-observed reflectivity within the cloud analysis. Then, during the diabatic forward model integration portion of the digital filter (and within the radar reflectivity region) the model-calculated temperature tendencies from the explicit microphysics scheme and cumulus parameterization are replaced by the temperature tendency derived from the radar reflectivity data.

Fig. 1 provides a schematic that illustrates the application of the latent heating based temperature tendency during the forward model portion of the DDFI. The diagnosis of the latent heating rate from the 3D radar mosaic and the NLDN data occurs within the RUC cloud analysis. First lightning ground stroke densities are used to supplement the reflectivity via a simple empirical formula. Then a latent heating rate proportional to the reflectivity intensity is found.

Information about the reflectivity and lightning data sources is as follows. The radar reflectivity used in the cloud analysis is from the NSSL national (CONUS) 3D radar mosaic grid with a 1-

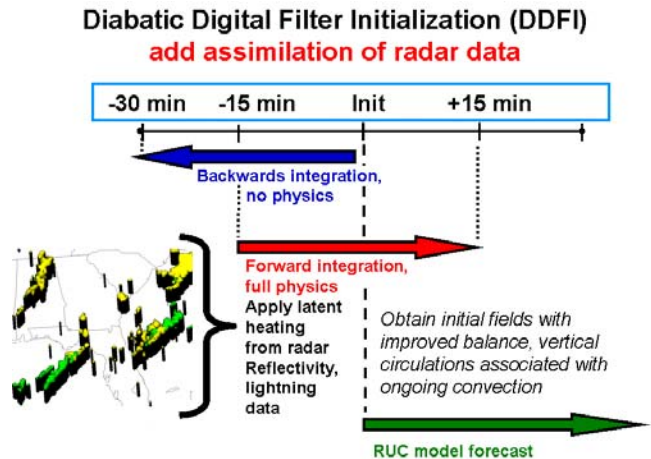


Fig. 7. Schematic diagram illustrating the application of the radar reflectivity-based latent heating within the diabatic digital filter initialization within the RUC model. In the sample plot, yellow and green shading show the contributions from the reflectivity and lightning data, respectively.

km horizontal resolution over 30 vertical levels and a 5-minute update cycle (Zhang et al. 2006). The data are generated by combining base level data from all available radars, performing quality control, and then combining reflectivity observations from individual radars onto a unified 3D Cartesian grid. The lightning ground stroke data is from the National Lightning Detection Network (NLDN) and can provide thunderstorm information in areas without radar coverage.

The RUC radar-enhanced DDFI method for initializing ongoing precipitation systems has a number of positive attributes. First, the method modifies the wind fields in a manner roughly consistent with the ongoing convection. Given the limitations of the observations, the horizontal grid resolution, and the parameterized representation of the convection, this is an appropriate objective. Numerous studies have shown that without modifying the wind field in this manner, the model retention of any assimilated hydrometeor information is short-lived.

Second, the modification of the wind field is done in a manner that minimizes shock to the model. Rather, the wind field evolves gradually during the DDFI to the prescribed heating rate. Note that the associated drying that would result is offset by increasing the water vapor in the reflectivity region within the cloud analysis. Third, the radar assimilation procedure requires no additional computer time, because the diabatic digital filter is already used to control noise in the RUC model initialization.

In addition to using the reflectivity data to prescribe latent heating temperature tendencies, radar reflectivity information is used to suppress model convection in areas with no echoes. In applying this convective suppression, it is extremely important to distinguish between regions with no echo and regions with no radar coverage. In these no coverage regions, the radar data cannot determine whether precipitation systems are ongoing and convective suppression is not warranted. The application of the convection suppression is as follows:

- 1) Determine a 2D “no echo” region, at least 100 km from any existing echo and excluding regions with no radar coverage.
- 2) During the DDFI and for the first 30 minutes of the model forecast, force a convective inhibition threshold condition that precludes the calling of the cumulus parameterization routine.

As a complement to the radar assimilation procedure, a suite of model simulated reflectivity fields have been added to the diagnostic fields available within the standard RUC model output

grab files. The available reflectivity fields include composite, and 1-km and 4-km AGL. The fields are derived using Z-Q relationships consistent with the Thompson microphysics scheme used in the RUC and a simple power law relationship to convert the parameterized precipitation into reflectivity. These fields were made available for forecast verification during the 2007 summer season. It is important to note that the model predicts grid average reflectivity over grid cell with a 13-km square horizontal projection. As such, verification of model predicted simulated reflectivity should utilize radar data that has been similarly averaged, or include a downscaling step to project the model reflectivity to an appropriately matched grid resolution.

By improving the RUC deterministic forecasts, the radar reflectivity assimilation procedure improved the RCPF forecast, however, a modification to the RCPF formulation is needed to take full advantage of the RUC improvements. This is because the RCPF has utilized the convective (sub-grid scale) precipitation as the convective predictor field, but with the reflectivity assimilation, actual convective now projects onto both the explicit and sub-grid scale RUC precipitation fields. This represents an improvement in the RUC as the larger convective systems should be at least partially resolved on the 13-km grid, but requires a modification to the RCPF algorithm for the RCPF to fully reflect the RUC improvement. After experimenting with using both parameterized and static stability thresholded grid-scale precipitation for the RCPF, a decision was made to use model simulated reflectivity. Use of either the explicit precipitation or the simulated reflectivity requires a static stability threshold check to assess whether the reflectivity / precipitation is convective in nature. Preliminary tests of an improved RCPF algorithm were completed during the summer of 2007, yielding encouraging results, but final determination of updated algorithm will be made in 2008.

Figs. 8 and 9 show a dramatic example of the RUC forecasts from the radar assimilation and the corresponding improvement in the RCPF when the new algorithm is applied to RUC forecasts with the radar assimilation. The case is dominated by two mesoscale convective systems. The first propagated southeastward from Northern Illinois into central Indiana, before weakening around 12z. The second system developed northwest of the first and was propagating southward across Central Illinois at 12z. The top panel of fig. 8 shows the RUC 3-h forecast 3-h accumulated precipitation valid 12z 17 July

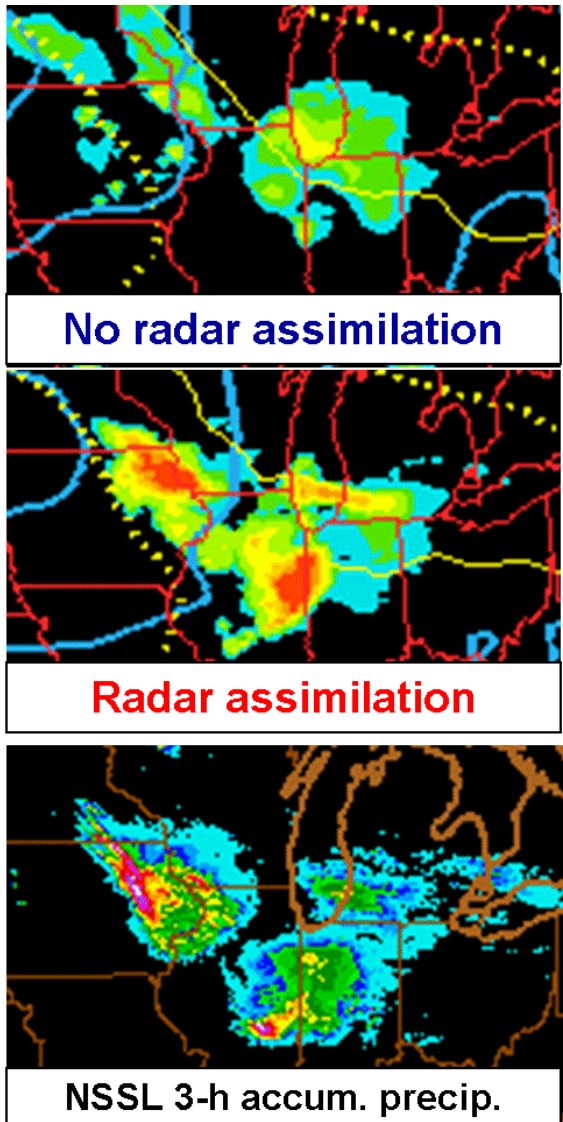


Fig. 8. 9z 17 July 2007 RUC 3-h forecast of 3-h accumulated precipitation valid 12z 17 July 2007 for case with reflectivity assimilation (top panel) and without reflectivity assimilation (middle panel). Verification (different color scale) in bottom panel.

2007. The middle panel shows the corresponding RUC forecast with the radar reflectivity assimilation and the bottom panel shows the NSSL 3-h estimated precipitation also valid 12z 17 July 2007. As can be seen, the radar assimilation results in a much better RUC 3-h precipitation forecast. Fig. 9 shows the associated RCPF forecasts. The top panel is from the RUC with the radar assimilation (middle panel in Fig. 8), but only using the convective precipitation as an RCPF predictor. The surprisingly poor performance of the RCPF formulation (despite the good RUC

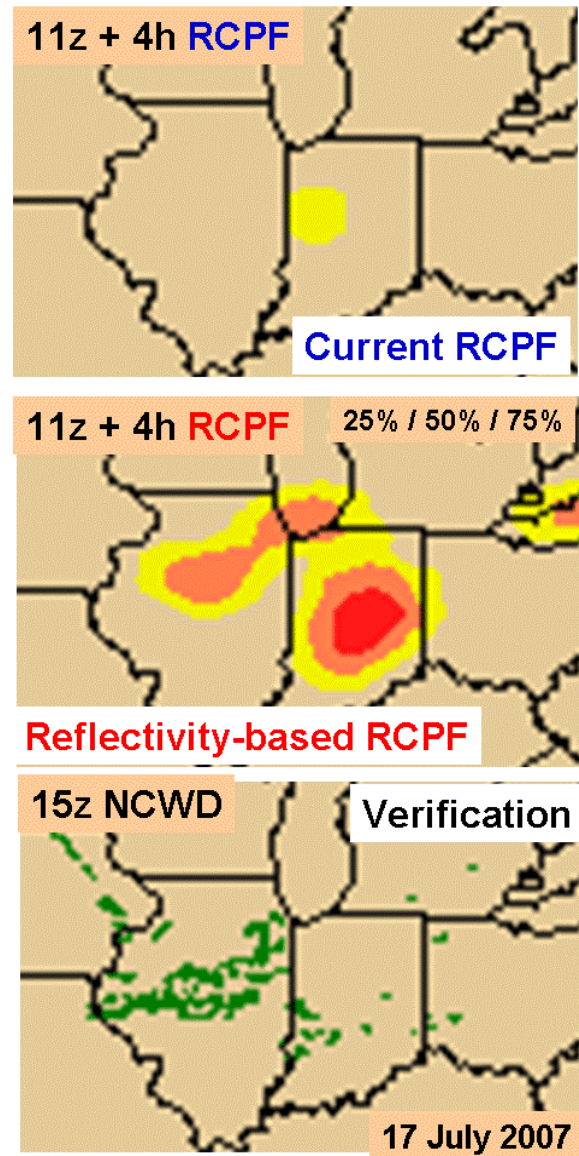


Fig. 9. 11z + 4h RCPF valid 15z 17 July 2007 from current convective precipitation-based formulation (top panel) and new reflectivity-based formulation. Both RCPF forecasts from the reflectivity assimilating RUC (middle panel in Fig. 8). 15z 4-km NCWD verification shown in bottom panel.

forecast) is due to the fact that most of the precipitation shown in the radar assimilation RUC forecast is explicitly resolved. The middle panel in Fig. 9 shows the RCPF from the RUC with the radar assimilation and the new algorithm that uses static stability thresholded simulated reflectivity. The bottom panel shows the NCWD 4-km depiction of convection. While the new RCPF is a significant improvement over the original, it still overpredicts the decaying MCS.

3.2 RCPF VERIFICATION

As previously noted RCPF grids and RUC simulated reflectivity fields were independently verified and evaluated during the summer of 2007. We show in this section our own verification comparison of the RCPF and CCFP from the verification sources available to us. These include the GSD RTVS verification of the CCFP (available via their web-site, presentation by Kay et al.), and our own verification for the RCPF. It is important to note that for all these verification, the RCPF was produced from the RUC forecasts with the radar assimilation, but the RCPF did not use the newer experimental algorithm based in static stability thresholded reflectivity. A significant change for 2007 verification was to replace the 40-km gridded NCWD verification with the raw 4-km gridded NCWD. This provided a more realistic depiction of the actual convective coverage (greatly reduced compared to the 40-km grids), resulting in a much more difficult forecast challenge and much higher forecast biases and lower CSI scores. CSI score differences (now much smaller) were still found to correlate with noticeable visual differences in respective forecasts.

Skill contour plots similar to Figs. 5 and 6 were created for both the RCPF and CCFP for the period 1 June – 31 Aug 2007 (not shown). They revealed similar patterns to those figs. with a few exceptions. Bias scores were significantly larger and CSI scores significantly reduced for all forecasts. Best average CSI verified against the 4-km grid are about .07 compared with about .24 for the 40-km NCWD verification. This does not reflect any fundamental change in the forecasts, just a difference in the verification metric. The biases for the CCFP were especially large during the daytime (average values in excess of 12), leading a reduction in relative forecast performance, especially for long lead times. RCPF biases were also too large, especially in the short-range morning forecasts, but less extreme than the CCFP. In contrast, short-range night-time CCFP forecasts (especially 2-h forecasts) showed very impressive skill (exceeding all other forecasts) and reasonable biases. Visual inspection of these forecasts suggests that this excellent performance was achieved by generally reducing the threat regions to compact polygons around ongoing nocturnal MCSs, and reducing forecasts of new nocturnal development. Fig. 10 shows the CSI and bias for the 6-h RCPF

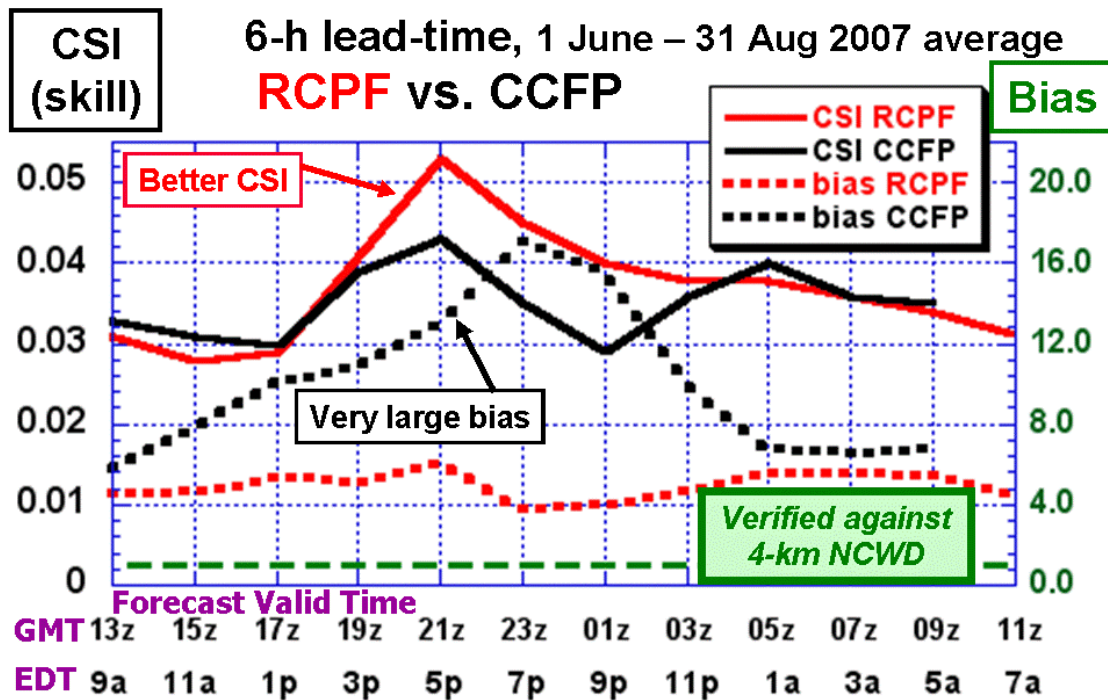


Fig. 10. Comparison of 8-h RCPF vs. 6-h CCFP (verified against 4-km NCWD) as a function of valid time for 3-month period (JJA) during 2007. CSI (solid lines – left side scale) and bias (dashed lines – right side scale) are shown for RCPF (red lines) and CCFP (black lines). For reference, bias = 1 lines is shown in long green dashes along bottom.

and CCFP forecasts averaged over the 3 month period (JJA). Note that consistent with its role as a guidance product to forecasters with an operational mission, the RCPF was provided in real-time to AWC. Also note that while not depicted in this comparison, the RCPF provides 1-h granularity in both the output frequency for a given forecast and the update frequency for new forecasts.

Clearly evident in Fig. 10 is the very large CCFP average bias during the daytime, which peaks at over 16 for the 17z + 6h forecast valid at 23z. This daytime period of very large CCFP biases (from 21z to 01z valid times) also corresponds with the period in which the RCPF scores significantly exceed the CCFP. At other times 6-h RCPF and CCFP CSI are similar. Fig. 11 shows the day-to-day variability in RCPF (red) and CCFP (blue) for 15z + 6h forecasts for August 2007. With some exceptions, RCPF scores tended to exceed CCFP during the middle of the month, with more similar scores near the beginning and end of the month. Also quite evident is the large day-to-day variability in scores for both forecasts and the similarity in relative skill, indicating some days present much harder forecast challenge than others.

A forecast example that illustrates these skill score differences is presented in Fig. 12. Shown are the CCFP 15z + 6h and RCPF 13z + 8h (accounting for the 2-h latency in the RCPF) forecasts valid 21z 19 Aug. 2007. Also depicted in green on the CCFP plot only is the NCWD 4-km verification. While both forecasts highlight similar regions for expected convection, the RCPF is more selective, yielding a better CSI score as shown in Fig. 11.

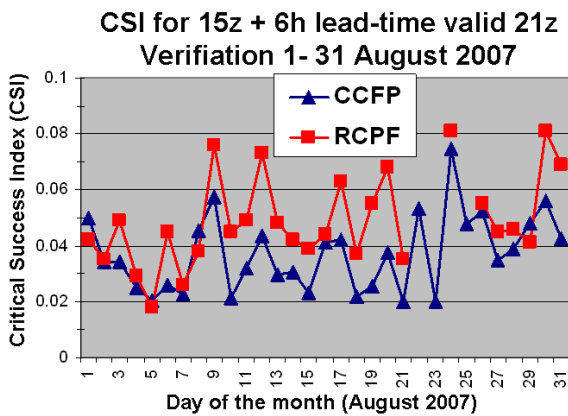


Fig. 11. Time series of CSI scores from 13z + 8h RCPF (red) vs. 15z + 6h CCFP (blue) valid 21z for the month of August, 2007.

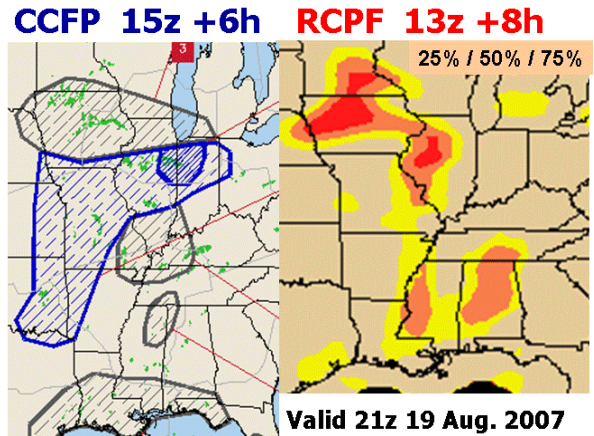


Fig. 12. Comparison of 15z + 6h CCFP and 13z + 8h RCPF valid 21z 19 August 2007. 4-km NCWD verification is shown on the CCFP plot.

3.3 EXPERIMENTAL HRRR FORECASTS

During the summer of 2007 we began limited experimental testing of 3-km High Resolution Rapid Refresh (HRRR) model predictions in support of coordinated efforts with NCAR and MIT/LL and NCEP toward a Coordinated Storm Prediction for Aviation (CoSPA) capability. Because the eventual operational CoSPA explicit thunderstorm-scale modeling system will require a radar assimilation procedure and at least hourly cycling to maintain the most accurate mesoscale environmental analysis, we envision the CoSPA HRRR as a natural evolution of the RUC and Rapid Refresh analysis and prediction system.

Our initial HRRR configuration was to utilize a small northeastern U.S. corridor domain (similar to the CIWS domain) that was manageable within our computer resources and covered the region of extremely high aviation impact from convective storms. An important and unique aspect of this prototype HRRR test system was the initialization of 3-km HRRR forecasts from the ESRL/GSD parallel version of the RUC cycle, which assimilates national radar reflectivity mosaic data via the diabatic DFI procedure described earlier, on an hourly basis. Thus the 3-km HRRR forecasts receive the full benefit of the hourly RUC assimilation, including the radar data assimilation.

Based on encouraging preliminary test case results, we began scheduled HRRR runs in August, 2007. The initial configuration included 12-h forecast every 3-h from the ESRL/GSD RUC with the radar reflectivity assimilation and 12-h forecasts from the NCEP operational RUC without the radar assimilation (it is scheduled for implementation

later in 2008). These latter runs were important for evaluating the impact of the RUC radar assimilation on the subsequent HRRR forecasts initialized from the RUC.

Qualitative evaluation of case study results (comparisons of the 3-km runs initialized from RUC runs with and without the reflectivity assimilation) has clearly demonstrated that the RUC reflectivity assimilation is effective at improving not only the RUC 13-km (with parameterized convection) forecasts (and related RCPF forecasts), but also the subsequent 3-km HRRR forecasts.

Figs. 13 and 14 illustrate this for a significant nocturnal MCS case from 16 Aug. 2007. Fig. 13 shows a comparison of the 1z + 2h CCFP with the 23z + 4h RCPF, both valid at 3z 16 Aug. The 23z RCPF had input from the 23z RUC forecast, which benefitted from radar assimilation of the reflectivity as the MCS was just initiating near Chicago (not shown). The resultant RCPF captured well the risk area, for this difficult to forecast case. Fig. 14 shows that the RUC reflectivity assimilation had an even more dramatic effect

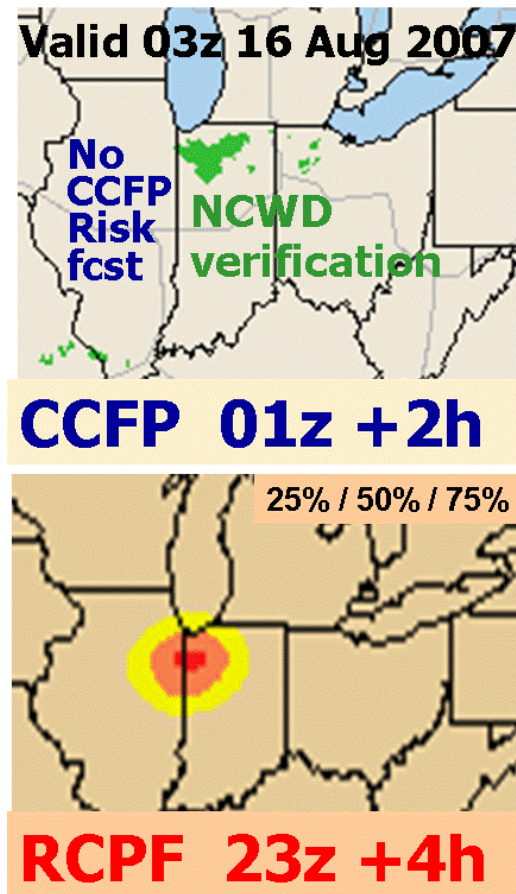


Fig. 13. Comparison of 1z + 2h CCFP and 23z + 4h RCPF valid 3z 16 August 2007. 4-km NCWD is shown.

on the subsequent 3-km HRRR forecast. Compared are the HRRR initialized from the 00z RUC with the reflectivity assimilation and a similarly configured 3-km run, initialized from the operational RUC without the reflectivity assimilation. This case illustrates the difference the reflectivity assimilation can make, especially for weakly forced convective system.

We conclude by showing a final case from a very high aviation impact day, 10 July 2007. On this day, a squall-line rapidly developed around 18z west of Chicago and propagated across O'Hare airport causing significant delays. As shown in Fig. 15, morning (11z) RCPF guidance for 19z was reasonable, but the corresponding CCFP forecast depicted 2 areas of possible convection across the upper Midwest, bracketing the actual position of the developing squall-line. The 11z RCPF forecast (available at 13z) included contributions from the 11z, 10z, and 9z RUC deterministic model runs. Reflectivity assimilation

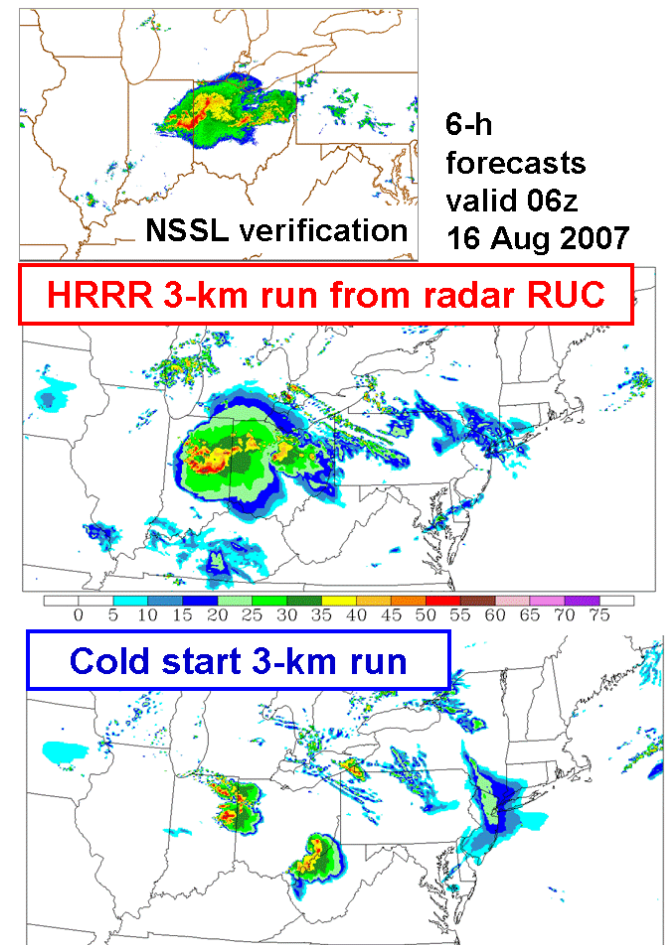


Fig. 14. Comparison of 6-h HRRR forecast reflectivity valid 6z 16 August 2007 - with (middle panel) and without (bottom panel) RUC reflectivity assimilation.

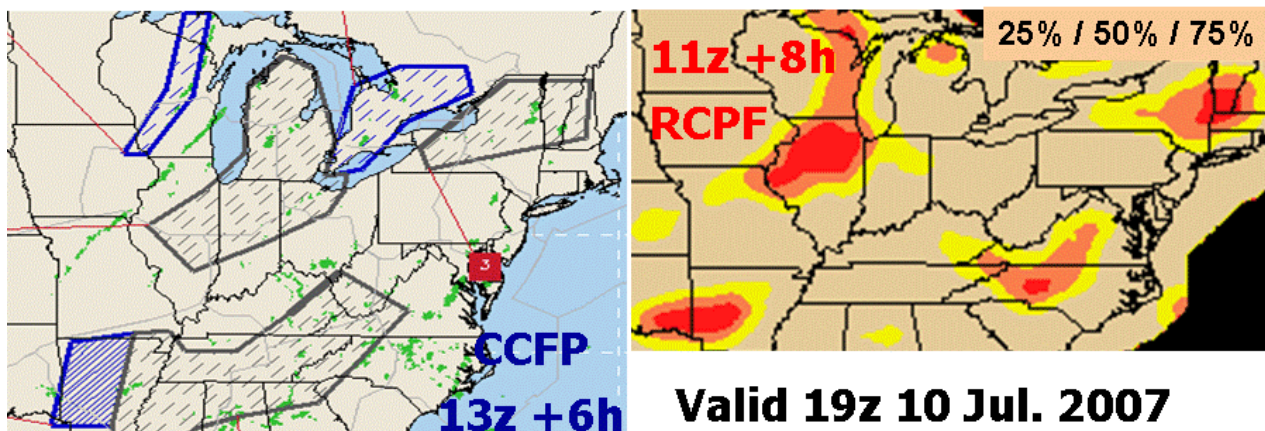


Fig. 15. Comparison of 13z + 6h CCFP and 11z + 8h RCPF valid 19z 10 July 2007. 4-km NCWD is shown on CCFP

was used in the runs, but was not a factor as there was no convection in the area at those times. RUC reflectivity assimilation began to become a factor for this squall-line at 17z, when the first echoes of the developing line appeared, but was much more significant by 18z. Fig. 16 shows a comparison of the 21z VIP level from MIT/LL and 18z + 3h HRRR forecasts initialized from both the RUC version with the reflectivity assimilation and the operational RUC version that does not yet have the reflectivity assimilation. While both provide reasonable overall forecasts of the convective evolution, the HRRR forecast initialized from the RUC with the reflectivity assimilation (middle panel) better captured the solid line approaching Chicago O'Hare airport, as well as a number of other convective features (storms in southern Illinois, southwestern Ohio, and Ontario).

4. Summary and outlook

We will continue development in the established research areas: 1) evolving the radar assimilation within the RUC to the Rapid Refresh, 2) continuing to optimize the RCPF and PETF. We will also pursue an expansion of our 3-km HRRR efforts as resources allow. We have done some preliminary experiments to evaluate the feasibility of producing hourly HRRR forecasts (initialized from the reflectivity assimilating RUC) with hourly output over a larger domain toward an eventual goal of a CONUS 3-km HRRR, with at least hourly cycling. In addition to value of the deterministic forecast from such a system, the potential value of probabilistic forecast from a time-lagged HRRR is very significant.

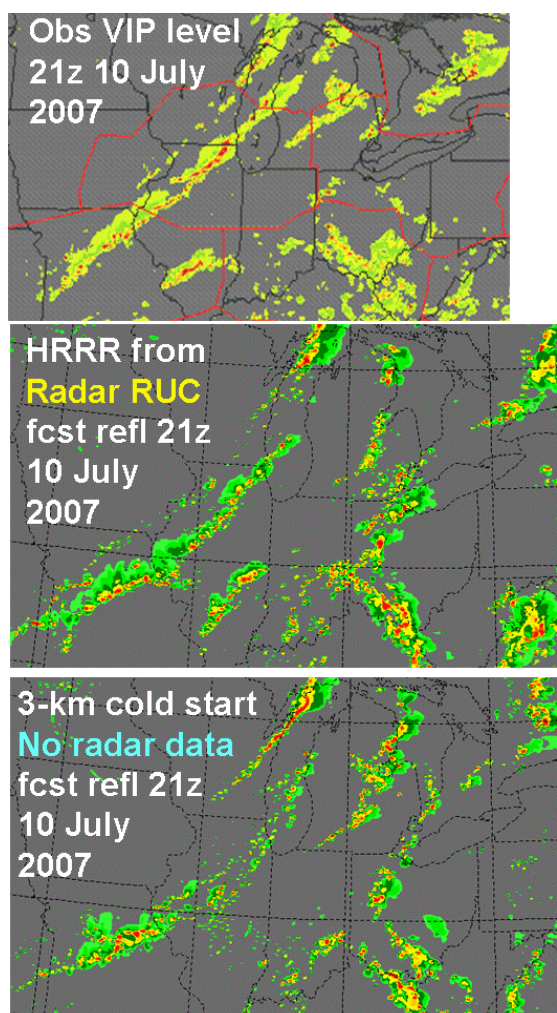


Fig. 16. Comparison of 3-h HRRR forecast reflectivity valid 21z 10 July 2007 – with (middle panel) and without (bottom panel) RUC reflectivity assimilation. VIP level verification is shown in top panel.

5. Acknowledgments

This research is in response to requirements and funding by the Federal Aviation Administration (FAA). The views expressed are those of the authors and do not necessarily represent the official policy or position of the FAA. In addition this work would not be possible without the FAA supported work of Jian Zhang and colleagues at NSSL to produce and distribute in real-time a quality controlled national radar reflectivity mosaic product.

6. References

- Benjamin, S., D. Devenyi, T. Smirnova, S. Weygandt, J. M. Brown, S. Peckham, K. Brundage, T. L. Smith, G. Grell, and T. Schlatter, 2006: From the 13km RUC to the Rapid Refresh. *12th Conference on Aviation Range and Aerospace Meteorology*, Atlanta, GA, American Meteorological Society, 9.1.
- Benjamin, S., and co-authors, 2007: From the radar enhanced RUC to the WRF-based Rapid Refresh. *18th Conf. Num. Wea. Pred.*, Park City, UT, AMS, J3.4.
- Benjamin, S. G., G. A. Grell, J. M. Brown, T. G. Smirnova, and R. Bleck, 2004a: Mesoscale Weather Prediction with the RUC Hybrid Isentropic/Terrain-Following Coordinate Model. *Monthly Weather Review*, **132**, 473-494.
- Benjamin, S. G., S. S. Weygandt, J. M. Brown, T. L. Smith, T. Smirnova, W. R. Moninger, and B. Schwartz, 2004b: Assimilation of METAR cloud and visibility observations in the RUC. *11th Conference on Aviation, Range, Aerospace and 22nd Conference on Severe Local Storms*, Hyannis, MA, American Meteorology Society, 9.13.
- Benjamin, S. G., D. Devenyi, S. S. Weygandt, K. J. Brundage, J. M. Brown, G. A. Grell, D. Kim, B. E. Schwartz, T. G. Smirnova, T. L. Smith, and G. S. Manikin, 2004c: An Hourly Assimilation/Forecast Cycle: The RUC. *Monthly Weather Review*, **132**, 495-518.
- Devenyi, D. and S. Benjamin, 2003: A variational assimilation technique in a hybrid isentropic-sigma coordinate. *Meteor. Atmos. Phys.*, **82**, 245-257.
- Devenyi, D., S. Weygandt, T. Schlatter S. Benjamin, and M. Hu, 2007: Hourly data assimilation with the Gridpoint Statistical Interpolation for Rapid Refresh. *18th Conf. Num. Wea. Pred.*, Park City, UT, AMS, 4A.2.
- Hu, M., S. Weygandt, M. Xue, and S. Benjamin, 2007: Development and testing of a cloud analysis package using radar, satellite, and surface cloud observations within GSI for initializing Rapis Refresh. *18th Conf. Num. Wea. Pred.*, Park City, UT, AMS, P2.5.
- Huang, X. and P. Lynch, 1993: Diabatic digital-filtering initialization: Application to the HIRLAM model. *Monthly Weather Review*, **121**, 589-603.
- Lynch, P. and X. Huang, 1992: Initialization of the HIRLAM model using a digital filter. *Monthly Weather Review*, **120**, 1019-1034.
- Thompson, G., R. M. Rasmussen, and K. Manning, 2004: Explicit Forecasts of Winter Precipitation Using an Improved Bulk Microphysics Scheme. Part I: Description and Sensitivity Analysis. *Monthly Weather Review*, **132**, 519-542.
- Weygandt, S., S. G. Benjamin, D. Dévényi, J. M. Brown, and P. Minnis, 2006a: Cloud and hydrometeor analysis using metar, radar, and satellite data within the RUC/Rapid-Refresh model. *12th Conference on Aviation Range and Aerospace Meteorology*, Atlanta, GA.
- Weygandt, S.S., S.G. Benjamin, J.M. Brown, and S.E. Koch, 2006b: Assimilation of lightning data into RUC model forecasting. *2nd Intl. Lightning Meteorology Conf.* Tucson, AZ
- Zhang, J., C. Langston, K. Howard, and B. Clarke, 2006: Gap-filling in 3D radar mosaic analysis using vertical profiles of reflectivity. *12th Conference on Aviation Range and Aerospace Meteorology*, Atlanta, GA.